Mathematical and Computational Applications, Vol. 15, No. 5, pp. 768-775, 2010.

EFFECT OF THE INITIAL DEFLECTION ON VIBRATION CHARACTERISTICS OF THE RUB-IMPACT ROTOR SYSTEM

Jiuhong Jia, Tianqi Hang

Key Laboratory of Pressure Systems and Safety, Ministry of Education
East China University of Science and Technology, 200237
Shanghai, P. R. China
jhjia@ecust.edu.cn

Abstract- Based on an elastic rub-impact model, a dynamic model of a rubbing rotor system with an initial deflection was set up and motion equations were derived and solved numerically. Poincaré maps, rotor orbits and bifurcation diagrams were drawn to investigate the effects of the initial deflection distance and the initial deflection angle on the vibration features of the rub-impact rotor system. The paper concluded that the initial deflection had great influence on the motion forms of the rubbing rotor system.

Keywords- Rotor System, Rub-impact, Initial Deflection, Vibration Features

1. INTRODUCTION

The rotor-stator rub is one of the main faults for large rotary machines, and lots of research work has been done by many researchers [1-5]. However, vibration characteristics of a rubbing rotor system with the initial deflection have rarely been studied especially in the published literatures. In this paper, a more general model of a rub-impact rotor system is set up in light of the elastic impact theory, so as to research the effect of the initial deflection on the vibration characteristics of a rubbing rotor system. Both the initial deflection length and the initial deflection angle are included in the model. Numerical calculation is utilized to solve the governing equations and the simulation results are given in the form of bifurcation diagrams, Poincaré maps and rotor orbits. Rotating speeds, the initial deflection length and the initial deflection angle are separately chosen as important parameters to carry out the research.

2. MATHEMATICAL MODEL OF THE RUBBING ROTOR SYSTEM

A two-degree-of-freedom model of a Jeffcott rotor system with the initial deflection is analyzed in this paper, as shown in Fig. 1. A disk of mass M, with an eccentricity e, is mounted on a massless flexible shaft and rotates inside the fixed stator with a clearance δ from the disk when there is no deflection for the shaft. Due to existence of the clearance between the rotor and the stator, the rotor may contact the stator intermittently during operation, causing complex dynamic behaviors.

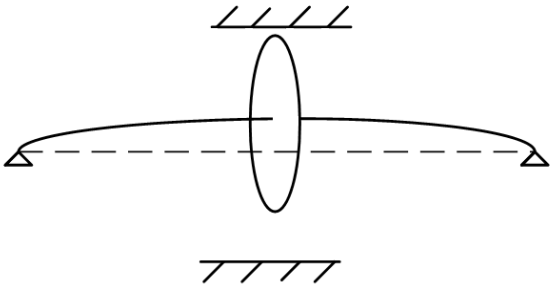

Fig.1 Schematic of the rub-impact rotor system model

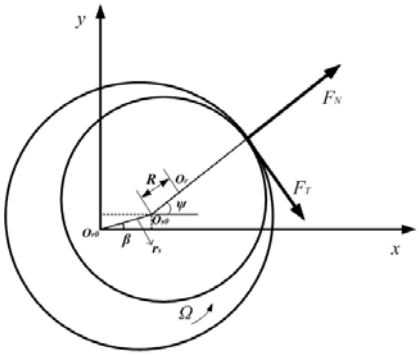

Fig.2 Schematic of the rub and impact forces

To derive governing motion equations, the co-ordinate system is chosen as shown in Fig. 2. In the static equilibrium, the center of the stator O_{s0} and the rotor center O_{r0} are separated by an initial deflection length r_s with an initial deflection angle β. Therefore, when the rotor is placed concentrically within the stator, $r_s = \beta = 0$.

According to the rubbing situation, the analysis of the rubbing rotor system can be divided into two stages. When the rotor center vibrates within the clearance δ, the rub doesn't happen. The main force exerting on the rotor is the elastic restoring force from the flexible shaft deformation. When the displacement of the rotor center is beyond the clearance, the rub happens. Then except for the elastic restoring force from the flexible shaft, due to the rub an elastic restoring force F_N from elastic deformation of the rotor and the stator, and a tangential frictional force F_T utilizing the model of Coulomb type of frictional force are also created and act on the rotor as shown in Fig. 2.

The radial rub force F_N and the tangential frictional force F_T can be expressed as

$$F_N(x,y) = \begin{cases} 0 & (for\ R < \delta) \\ (R-\delta)K_s & (for\ R > \delta) \end{cases} \qquad F_T = \mu F_N \tag{1}$$

where μ is the friction coefficient between the rotor and the stator, K_s is the stator stiffness, and $R = \sqrt{(x-x_0)^2 + (y-y_0)^2}$. And (x_0, y_0) is the coordinate of the stator center with $x_0 = r_s \cos\beta$, and $y_0 = r_s \sin\beta$.

In the *oxy* co-ordinate system, the dynamic governing equations for the rubbing system are:

$$M\ddot{x} + c\dot{x} + F_x = Me\Omega^2 \cos(\Omega t + \alpha) \tag{2}$$

$$M\ddot{y} + c\dot{y} + F_y = Me\Omega^2 \sin(\Omega t + \alpha) \tag{3}$$

When $R < \delta$

$$F_x = KR\cos\psi + Kx_0 \tag{4}$$

$$F_y = KR\sin\psi + Ky_0 \tag{5}$$

where K is rotor stiffness, $\cos\psi = (x - x_0)/R$, and $\sin\psi = (y - y_0)/R$.

When $R \geq \delta$

$$F_x = -F_N\cos\psi + F_T\sin\psi = -K_s(1-\delta/R)[(x-x_0) - \mu(y-y_0)] \tag{6}$$

$$F_y = -F_N\sin\psi + F_T\cos\psi = -K_s(1-\delta/R)[\mu(x+x_0) + (y+y_0)] \tag{7}$$

When nondimensionalized, the governing equations are as follows.

When $\hat{z} < 1$, the rub between the rotor and stator doesn't happen. The governing equations are:

$$\hat{x}'' + 2v\hat{x}' + \hat{x} = \varepsilon\omega^2\cos(\omega T + a) \tag{8}$$

$$\hat{y}'' + 2v\hat{y}' + \hat{y} = \varepsilon\omega^2\sin(\omega T + a) \tag{9}$$

When $\hat{z} \geq 1$, the rub happens. The governing equations are:

$$\hat{x}'' + 2v\hat{x}' + \hat{K}(1-1/\hat{z})[(\hat{x}-\hat{x}_0) - \mu(\hat{y}-\hat{y}_0)] = \varepsilon\omega^2\cos(\omega T + a) \tag{10}$$

$$\hat{y}'' + 2v\hat{y}' + \hat{K}(1-1/\hat{z})[\mu(\hat{x}-\hat{x}_0) + (\hat{y}-\hat{y}_0)] = \varepsilon\omega^2\sin(\omega T + a) \tag{11}$$

in which, $\omega_0 = \sqrt{K/M}$ is the undamped natural frequency of the rotor system, Ω the rotor rotating speed, $\omega = \Omega/\omega_0$, $T = \omega t$, $' = d/dT$, $v = c/2\omega_0 M$, $\hat{x} = x/\delta$, $\hat{y} = y/\delta$, $\hat{z} = R/\delta = \sqrt{(x-x_0)^2 + (y-y_0)^2}/\delta = \sqrt{(\hat{x}-\hat{x}_0)^2 + (\hat{y}-\hat{y}_0)^2}$, $\varepsilon = e/\delta$, $\hat{x}_0 = x_0/\delta$, $\hat{y}_0 = y_0/\delta$, $\hat{K} = K_s/K$, and c the damping.

3. NUMERICAL SIMULATION AND ANALYSIS

Since the nondimensional governing motion equations have been obtained above, they are transferred into a set of first order differential equations $\dot{u} = f(u)$. Then the fourth-order Runge-Kutta method is used to integrate this set of equations. According to the analysis need, some parameters can be used as the control parameters such as the rotor rotating speed, and the initial deflection, while other parameters keep fixed during every time of calculation. To get the stable result, a small integration step has to be chosen to avoid the numerical divergence at the point where derivatives of F_x and F_y are discontinuous. In this paper, the integration step is chosen to be $2\pi/500$, i.e., within one period, there are 500 times of integral calculation. Generally, long time marching computation is required to obtain convergent values. During every calculation, results of the first 500 periods are abandoned, and then results of the next 100 periods are chosen to carry out various kinds of analysis. To study effect of the initial deflection on vibration characteristics of the rubbing rotor system, bifurcation diagrams, Poincaré

maps and rotor orbits are employed. They are all useful and effective ways to illustrate the motion behaviors of the rotor system.

3.1. Effect of the Initial Deflection Length

The parameters used during the computations are $v = 0.1096$, $\hat{K} = 6.667$, $\varepsilon = 0.6$, $\beta = \pi / 2$, and $\alpha = 0.0$. Bifurcation diagrams, Poincaré maps and rotor orbits using the initial deflection length r_s / δ as the control parameter at different rotating speed ratios ω are drawn and analyzed as in Fig.3-Fig.8.

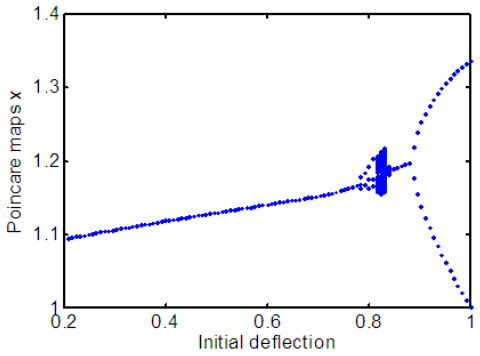

Fig.3 Bifurcation diagram with $\omega = 1.2$

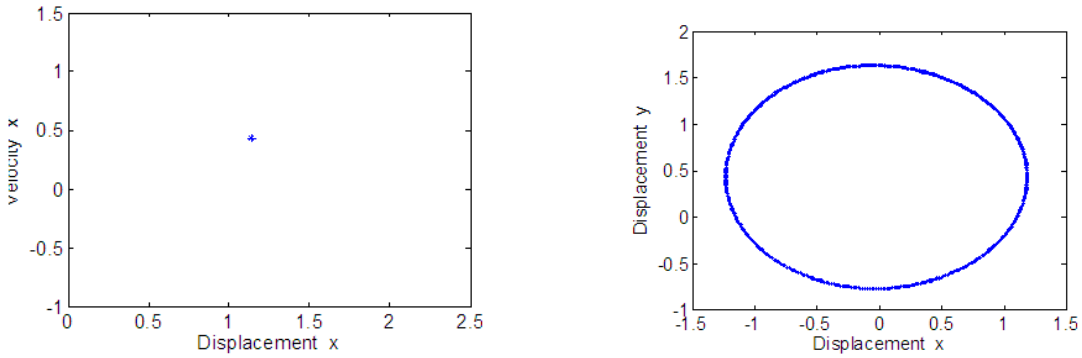

Fig.4 Poincaré map and rotor orbit when $\omega = 1.2$ and $r_s / \delta = 0.6$

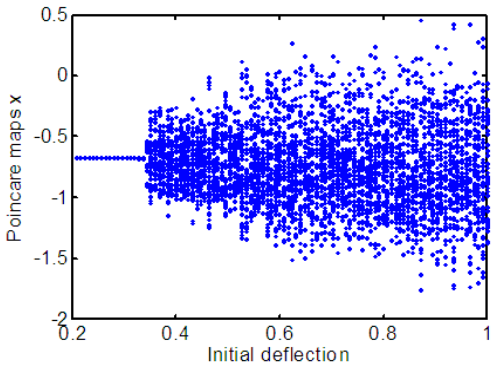

Fig.5 Bifurcation diagram with $\omega = 2.8$

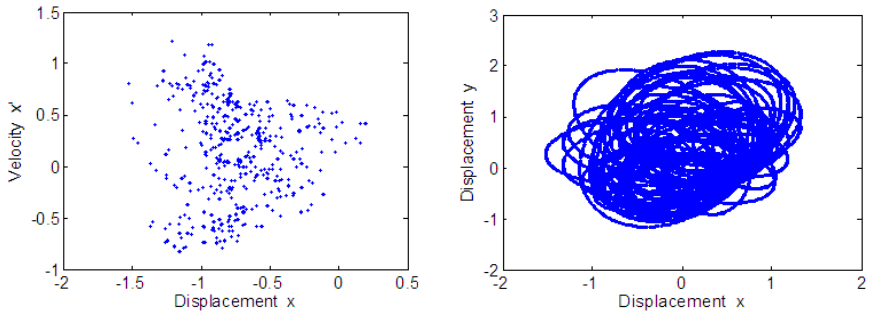

Fig.6 Poincaré map and rotor orbit when $\omega = 2.8$ and $r_s / \delta = 0.6$

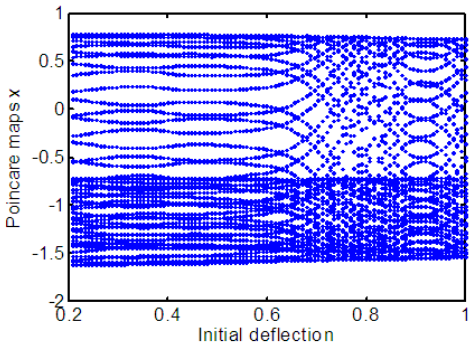

Fig.7 Bifurcation diagram with $\omega = 4.8$

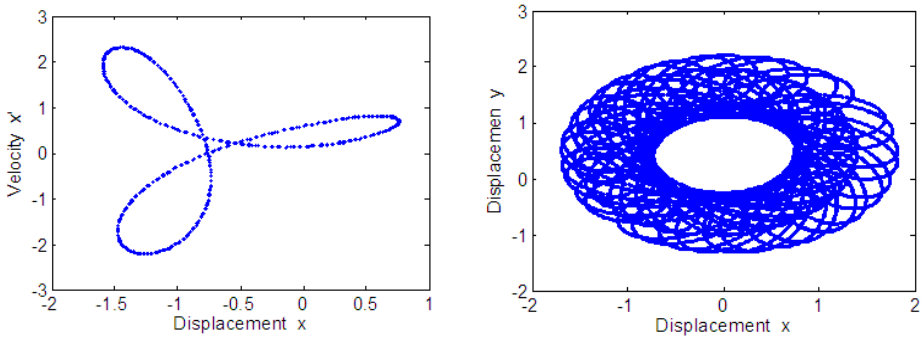

Fig.8 Poincaré map and rotor orbit when $\omega = 4.8$ and $r_s / \delta = 0.6$

From above figures, it's obvious that under different rotor rotating speeds, the bifurcation diagrams using the non-dimensional initial deflection length r_s / δ as the control parameter are quite different. When the speed is low as shown in Fig.3 , with ω =1.2 and within the range r_s / δ =0.2-1.0, the motion is synchronous with period-1 as illustrated in Fig.4 in detail, where Poincaré map is an isolated point and the rotor orbit is a circle. This periodic motion means that the rub doesn't happen with these system parameters. When the initial deflection length further increases and reaches about 0.8, the bifurcation phenomenon happens and the motion changes from synchronous period-1 to period-3 and even becomes chaotic. After that, the motion return period-1 and eventual period-2. With the increase of the rotor speed as ω ＝2.8 in Fig.5, comparing Fig.5 with Fig.3, it is obvious that the period-1 motion range becomes smaller. When r_s / δ reaches about 0.35, the period-1 motion becomes

chaotic as further explained in Fig.6, where Poincaré map has fractal structure and the orbit is irregular. Under the high speed like ω=4.8 in Fig.7, the motion has no periodic stage and always keeps quasi-periodic and even chaotic as shown in Fig.8, where Poincaré map is a closed circle which means the motion is quasi-periodic.

3.2. Effect of the Initial Deflection Angle

The parameters used during the computations are $v = 0.1096$, $\hat{K} = 6.667$, $r_s = 1.0$, $\varepsilon = 0.6$, and $\alpha = 0.0$. Using the rotating speed ratio as the control parameter, the bifurcation diagrams, Poincaré maps and rotor orbits with different initial deflection angles are drawn and analyzed as in Fig.9-Fig.14.

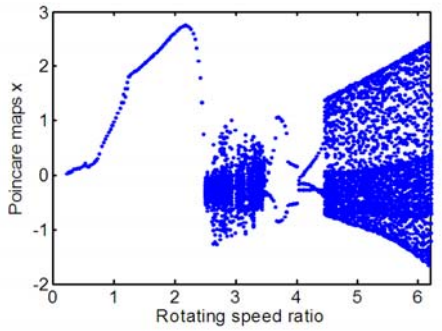

Fig.9 Bifurcation diagram with $\beta = 0.0$

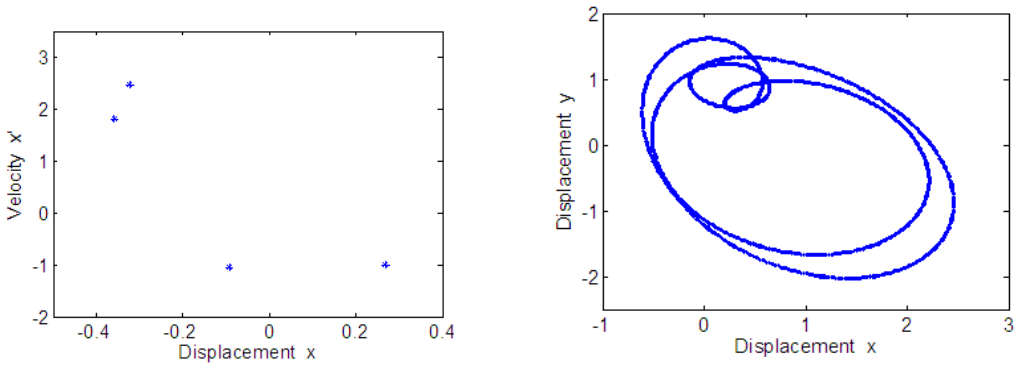

Fig.10 Poincaré map and rotor orbit when $\omega = 3.5$ and $\beta = 0.0$

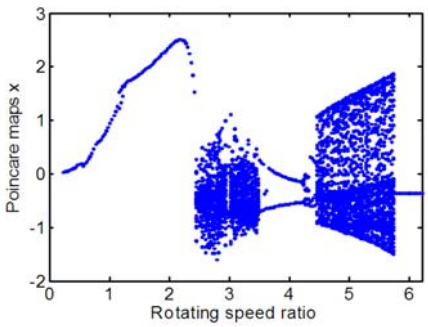

Fig.11 Bifurcation diagram with $\beta = \pi / 4$

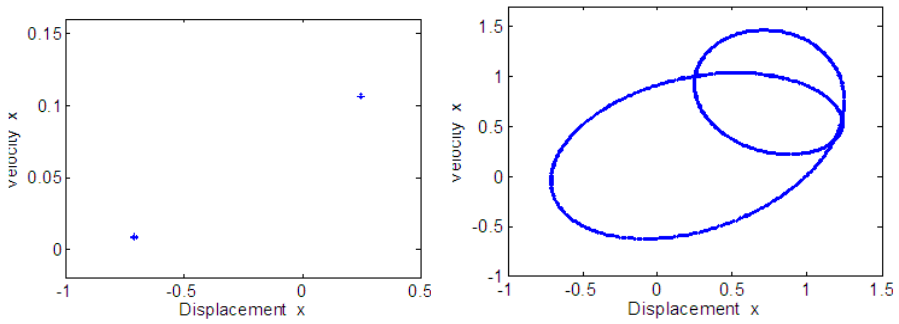

Fig.12 Poincaré map and rotor orbit when $\omega = 3.5$ and $\beta = \pi / 4$

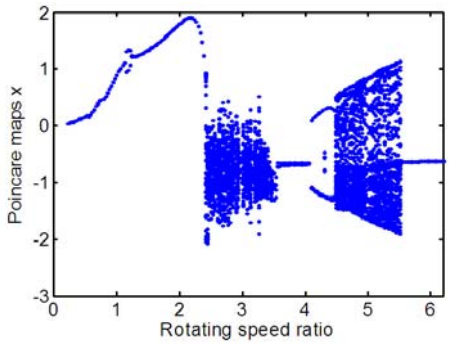

Fig.13 Bifurcation diagram with $\beta = \pi / 2$

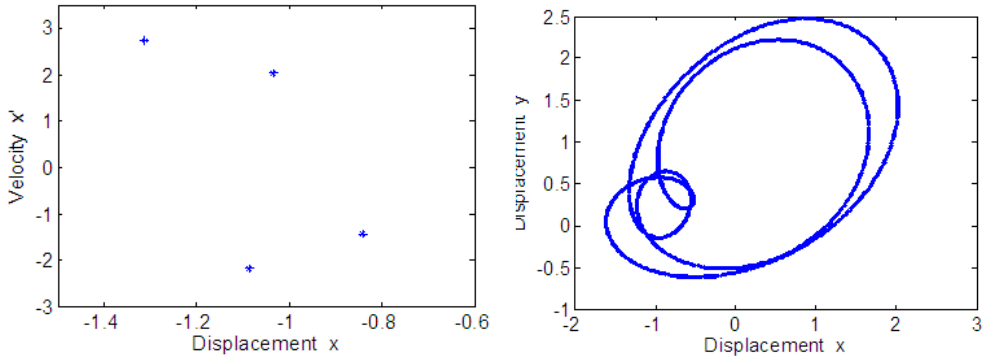

Fig.14 Poincaré map and rotor orbit when $\omega = 3.5$ and $\beta = \pi / 2$

Fig.9, Fig.11 and Fig.13 are bifurcation diagrams using the rotor speed as the control parameter with various initial deflection angles β =0.0, $\pi / 4$ and $\pi / 2$ respectively. Due to different initial angles, different forms of motions can be clearly seen in these diagrams.

In Fig.9, within the speed range ω =0.2-2.45, the motion is synchronous with period-1. However, in Fig.11 and Fig.13, especially in Fig.13 when ω is about 1.2, there is an obvious bifurcation phenomenon, where the motion changes from period-1 to period-2 and then period-1 again. In these three figures, for the range ω =3.5-4.5, the motions are also quite different. For detailed analysis, when ω =3.5 for $\beta = 0.0$, the motion is synchronous with period-4 as further illustrated in Fig.10, where the Poincaré map has four isolated points and the rotor orbit has four closed circles. When ω =3.5

for $\beta = \pi / 4$, the motion is synchronous with period-2 which can be proved in Fig.12, where the Poincaré map has two isolated points and the rotor orbit has two closed circles. When ω＝3.5 for $\beta = \pi / 2$, as shown in Fig.14, the motion is also synchronous with period-4, but the rotor orbit shape is different with the one in Fig.10. There is one big difference for these three bifurcation diagrams. For $\beta = 0.0$ after ω＝3.5, the motion keeps chaotic. While for $\beta = \pi / 4$ and $\beta = \pi / 2$, after ω＝5.8, the motion changes from chaotic style to period-1.

4. CONCLUSIONS

(1) Based on the classic impact model, the rubbing rotor model with the initial deflection is set up, the governing equations are derived and finally the numerical simulation is carried out for the analysis of effect of the initial deflection on vibration characteristics of the rubbing rotor system.

(2) From the analysis, with different initial deflection lengths, when the rotor rotating speed is low, the motion is synchronous with period-1 until the initial deflection becomes too large, leading to bifurcation and chaotic motions. With the increase of the speed, the rubbing begins to happen under smaller speeds, and the motion becomes quasi-periodic and even chaotic.

(3)With different initial deflection angles, the system motion styles are quite different, which proves that the initial deflection angle has big influence on the rubbing rotor system.

5. ACKNOWLEDGEMENTS

The author is grateful for the support of the funds (No. 50905059 and No：20090074120005). Great thanks also give to Professor Shantung Tu for his useful instructions and Dr. Xiaoyao Shen for his fruitful suggestions.

6. REFERENCES

1. Z. G. Sun and J. X. Xu, Analysis on complicated characteristics of a high-speed rotor system with rub-impact, *Mechanism and Machine Theory* **37**, 659-672, 2002.
2. F. L. Chu and Z. S. Zhang, Periodic, quasi-periodic and chaotic vibrations of a rub-impact rotor system supported on oil film bearings, *International Journal of Engineering Science* **35**, 963-973, 1997.
3. M. Karlberg and J. O. Aidanpaa, Numerical investigation of an unbalanced rotor system with bearing clearance, *Chaos, Solitons and Fractals* **18**, 653-664, 2003.
4. J. Zapomel and C. H. J. Fox, Numerical investigation of a rotor system with disc-housing impact, *Journal of Sound and Vibration* **243**, 215-240, 2001.
5. S. Edwards and A. W. Lees, The influence of torsion on rotor/stator contact in rotating machinery, *Journal of Sound and Vibration* **225**, 767-778, 1999.